10.1109/ICRA.2015.7139423

Closed Loop Task Space Control of an Interleaved Continuum-Rigid Manipulator

Benjamin Conrad and Michael Zinn, *Member, IEEE*

***Abstract*— A new manipulation approach, referred to as interleaved continuum-rigid manipulation, which combines inherently safe, flexible actuated segments with more precise embedded rigid-link joints has recently been introduced** [1], [2]**. The redundantly actuated manipulator possesses the safety characteristics inherent in flexible segment devices while gaining some of the performance attributes of rigid-link joint systems. In this paper, we describe a general controller developed for an interleaved manipulator. The controller is implemented on a clinically-relevant prototype, the results of which demonstrate the advantages of an interleaved manipulator. We also consider kinematic drivers of the interleaved manipulator workspace, showing that careful kinematic considerations can substantially improve manipulator workspace and task accuracy.**

I. Introduction

Minimally-invasive surgical (MIS) robotic systems can be classified as either rigid-link manipulators, such as Intuitive Surgical's Da Vinci [3], or flexible continuum manipulators, such as Hansen Medical's Artisan catheter system [4] and Stereotaxis' Niobe [5]. The primary advantage of the flexible manipulator approach is its superior safety characteristics as compared to rigid manipulators. A compliant structure makes these manipulators much less likely to cause damage when they come in contact with tissue, leading to their dominance in applications where safety is of particular concern, such as in intracardiac interventional procedures. While MIS systems based on flexible robotic manipulators have met with success, the very features which enable their superior safety characteristics have hindered their use in high performance manipulation tasks. Their soft compliant structure, in combination with the internal friction inherent to their design, results in poor position [6], [7] and force regulation, limiting their use to simpler surgical procedures.

A number of researchers have investigated alternative continuum design approaches, deviating from the tendon-actuated continuum thermoplastic designs found in the vast majority of commercially available flexible medical devices, such as catheters. In general, these approaches have sought to improve performance while maintaining the device's small size and ability to navigate complex paths. In [8]–[10] a novel concentric tube design is used to achieve a very small device cross-section, facilitating access to small anatomical features. In this case, while device compliance can be kept low, the fundamental trade-off between compliance (for safety) and performance still limits positioning accuracy. In [11]–[13], a highly articulated, redundant robot probe provides a high degree of maneuverability while maintaining the proximal shape of the probe and thus reducing the chance of injury to sensitive tissue. However, this design approach employs relatively stiff and/or rigid-link construction, potentially compromising the inherent safety embodied by the compliant manipulator concept.

Recently, the use of feedback and associated sensing of flexible MIS robotic manipulators has been explored by a number of investigators to improve the performance of inherently safe flexible continuum manipulators. In [14] a closed loop system was developed to control end-point position in both task space and joint space. Other examples include [15] where tracking of beating heart motion is explored, [8], [16] where concentric tube manipulators are controlled in position and end-point stiffness and [7], [11], [17]–[26] where various specialized control applications are investigated. Fundamentally, the inherent flexibility and internal friction of flexible continuum manipulators, such as cardiac intervention catheters, result in nonlinear hysteresis behavior that limits the closed loop bandwidth. This, in turn, compromises the system's ability to reject disturbances on the desired time scales. In addition, the nonlinear, non-stationary motion characteristics of these compliant devices often result in limit cycling when used in closed loop control, reducing the effectiveness of feedback approaches. This is particularly difficult to address for multi-degree-of-freedom manipulators where the hysteresis-induced nonlinear motion is complex and difficult to predict.

II. Interleaved Manipulation

While the design and feedback approaches previously investigated have provided improvements in the performance of flexible continuum manipulators, none have achieved the performance levels typical of rigid-link designs while maintaining the compliant, atraumatic manipulator characteristics preferred for safety critical applications. The authors believe that the difficulty in achieving both inherent safety and performance is due to fundamental limitations

*Partial funding for this research was provided by the National Science Foundation under Grant No. IIS-1316271.

Benjamin Conrad is a graduate student with the Mechanical Engineering Department, University of Wisconsin – Madison, Madison, WI 53706 USA (e-mail: bconrad@wisc.edu)

Michael Zinn is with the Mechanical Engineering Department, University of Wisconsin – Madison, Madison, WI 53706 USA (phone: 608-263-2893; fax: 608-265-2316 e-mail: mzinn@wisc.edu)

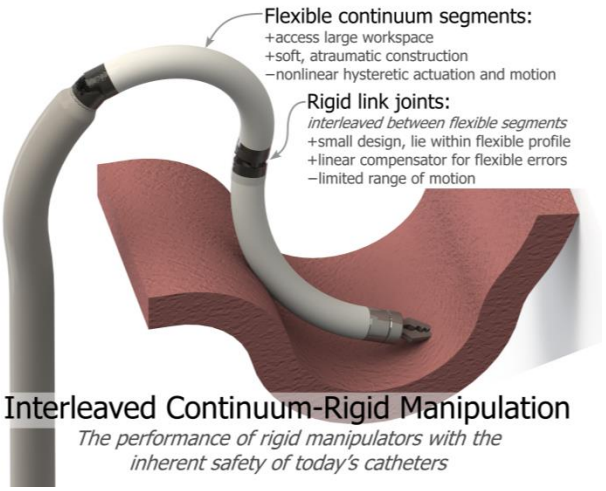

Figure 1. Overview of Interleaved Continuum-Rigid Manipulation.

that exist when working with flexible continuum manipulators.

To overcome these challenges we have proposed a new approach to continuum robotic manipulator design and actuation – where the safety advantages of flexible continuum manipulators are merged with the performance advantages of traditional rigid-link manipulators [2]. The approach in Fig. 1 advocates the combination of flexible, actively actuated continuum segments with small, rigid link actuators. The small rigid-link joints are interleaved between successive continuum segments and provide a redundant motion capability. The authors refer to this approach as *interleaved continuum-rigid manipulation* (see [1], [2]). The active continuum segments provide large motion capability through, for example, a combination of tendon-driven articulation and telescoping motion. The compliant atraumatic construction of the continuum segments enhance safety, while the small size of the rigid-link joints allows both the joint and actuator to be embedded inside the profile of the compliant segments. Limiting the rigid link joint stroke allows the joints to assume a compact form, allowing for the use of a wide variety of micro-scale actuation concepts. The repeatable, predictable motion of the small actuators allows for active correction of motion errors. The introduction of the small rigid joints is central to the overall concept – in that they act as *linearizing* elements in a system whose overall behavior is highly nonlinear – thus allowing for effective use of feedback control to enhance performance.

III. Kinematics

A. Interleaved Kinematics

The kinematic description of an interleaved manipulator closely resembles the physical arrangement, having the general form of

$$T(q_1 \dots q_n) = (T_r(q_1))_1 \left(T_f(q_2)\right)_2 \dots \left(T_f(q_{n-1})\right)_{n-1} (T_r(q_n))_n, \quad (1)$$

where $(T_r)_i$ is the homogeneous transformation matrix for the i^{th} rigid link joint having joint position q_i, and similarly $(T_f)_j$ represents the j^{th} flexible segment. The joint transformation matrices are particular to each joint design; examples of rigid joint matrices can be found in any robotics text (e.g. [27]) while [2] and [6] derive the kinematics of flexible articulating sections. Note that the resulting transformation matrix, *T*, is a kinematic description and therefore does not include any nonlinearities due to joint friction, deformation, or other common occurrences.

B. Kinematic Design Considerations

The kinematic design and specific device mechanical design details will have a significant effect on the performance of the manipulator. It is useful to explore both in the context of the interleaved approach. As described earlier, one of the functions of the rigid link joints is to compensate for flexible segments motion errors. As such, the task space motion bounds of the rigid link joints should envelope the task-space error bounds of the flexible segments.

The task space error can be evaluated as:

$$\Delta x_f \cong J_f \Delta q_f \quad (2)$$

where J_f is the flexible segment Jacobian and Δq_f is the flexible segment joint space motion errors. The task space error, Δx_f, at a given configuration is evaluated by mapping the joint space error bounds to task space using equation (2). Similarly, the task space motion due to the motion of the rigid link joints can be evaluated as:

$$\Delta x_r \cong J_r \Delta q_r \quad (3)$$

where J_r is the rigid link joint Jacobian and Δq_r is the rigid link task space motion. Using (2) and (3), the flexible segment task-space error bounds can be evaluated from the joint space error bounds and the rigid link task space motion bounds can be evaluated from the rigid link joint limits (see Fig. 2). By comparing the error and motion bounds, we can evaluate the regions where the motion error due to the flexible segments can and cannot be corrected by the rigid link joint motion (see Fig. 2)

An example two degree of freedom manipulator, overlaid with the error and motion bounds of the flexible and rigid link joints respectively, is shown in Fig. 3. The regions of uncorrectable error are a function of the rigid link joints' range of motion, the error ranges of the flexible segments, and the configuration of the manipulator.

Alternatively, we can evaluate the rigid link joint motions required to fully correct for the flexible segment motion errors. In this case, the required rigid link joint motions are evaluated by equating equations (2) and (3) and solving for Δq_r

$$\Delta q_r \cong J_r^{-1} J_f \Delta q_f \,. \quad (4)$$

To evaluate the required rigid link joint motion to compensate for all possible flexible segment errors at a given configuration, equation (4) can be used to map the set of flexible segment joint errors limits to the set of corresponding required rigid link joint motions – the

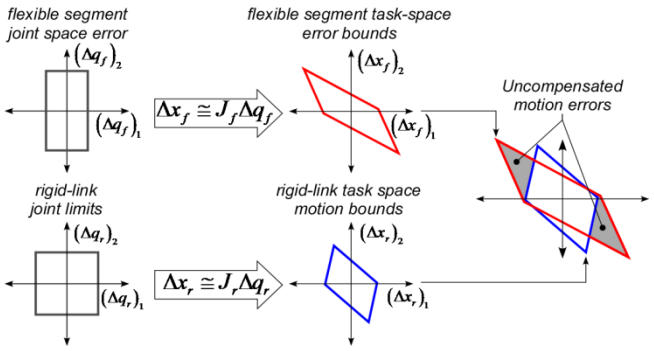

Figure 2. Flexible segment and rigid-link task-space error and motion bounds for a two degree-of-freedom manipulator.

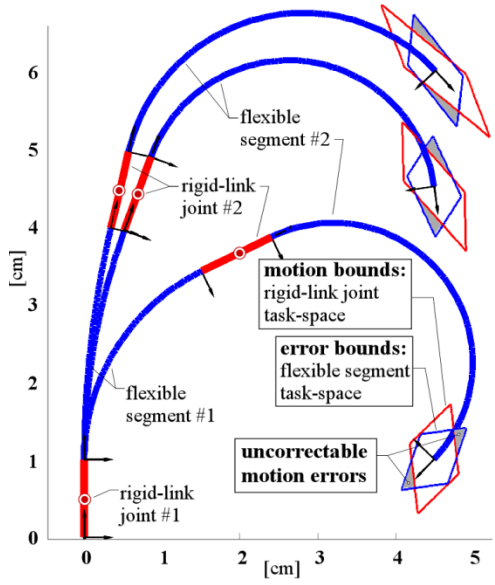

Figure 3. Task-space error and motion bounds of the flexible segment and rigid-link joints. The proximal and distal flexible segment articulation errors depicted are ±0.15[rad]. The rigid-link joint range of motion depicted are ±0.10[rad].

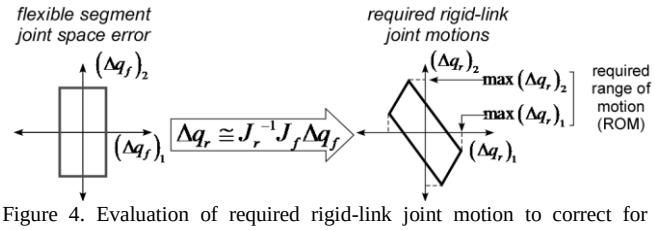

Figure 4. Evaluation of required rigid-link joint motion to correct for flexible segment motion errors.

maximum of which corresponds to the required rigid link joint range of motion (RoM) to compensate for all possible errors at the specified configuration (see Fig. 4).

Using the two degree-of-freedom example introduced previously, we can see how the required rigid link joint RoM varies as a function of manipulator configuration. In this case, we make the assumption that the flexible segment joint motion errors (defined as deviations in the flexible segment curvature) are proportional to the magnitude of the flexible segment curvature. This assumption is based on prior catheter modeling and experimental data given in [6] and is due to the increased tendon friction forces (and resulting error in curvature) that occur with high segment curvature. As shown in Fig. 5, the required rigid link RoM (to fully compensate for the flexible segment errors) is a strong function of segment curvature and thus varies considerably over the workspace of the device. The required RoM is largest in configurations where both segments have high curvature – resulting in large flexible segment errors.

In Fig. 6, the required RoM for the rigid link joint #2 is generally larger than the RoM for joint #1. However, as the manipulator's nominal configuration is varied the rigid link's required RoM varies as well. For instance, if the nominal position of the rigid link joint #2 is set to 90 degrees, then the required rigid link joint RoM (to compensate for flexible segment errors) changes significantly (see Fig. 6). In this case, the required rigid-joint RoM is generally less than that shown in the prior example, where the nominal rigid link joint positions were

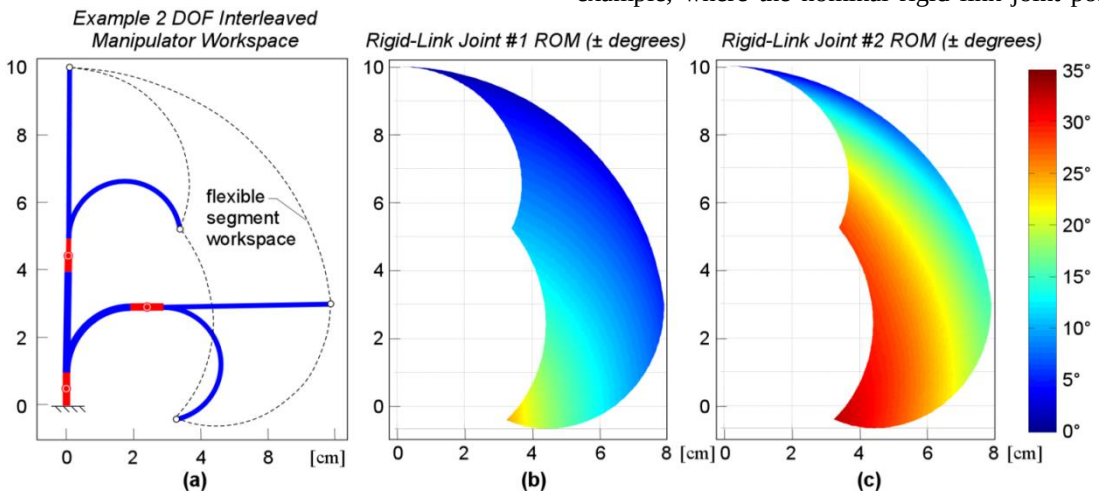

Figure 5. Required minimum rigid-link joints range of motion (RoM) to fully compensate for flexible segment motion errors as a function of manipulator configuration. The nominal angle of the rigid-link joints is set equal to zero and the flexible segment joint limits, given in segment curvature, are [0 to 0.5] and [0 to 0.6] cm for segments #1 and #2, respectively ([0° to 90°] and [0° to 170°] of articulation. The flexible segment joint motion errors are assumed to be proportional to the magnitude of the flexible segment joint motions (in this case we assume a ±20% variation of flexible segment curvature). (a) Two degree-of-freedom interleaved manipulator (flexible segment) workspace. (b) Contour plot of rigid-link joints #1 required RoM over complete workspace. (c) Contour plot of rigid-link joints #2 required RoM over complete workspace.

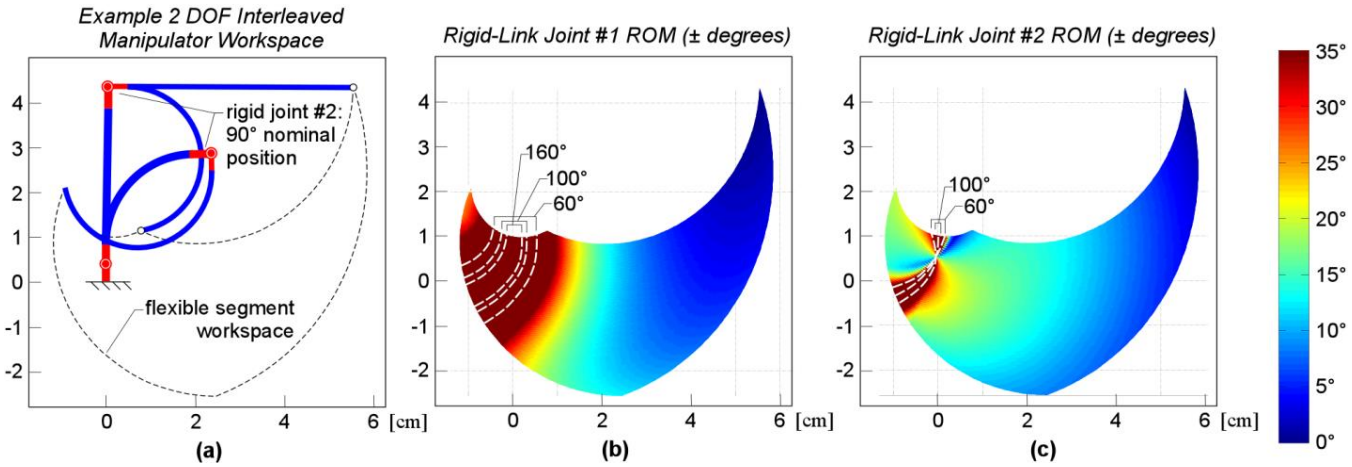

Figure 6. Required minimum rigid-link joints range of motion (RoM) to fully compensate for flexible segment motion errors. The nominal angle of the rigid-link joint #1 and #2 are set equal to 0.0 and 90°, respectively. The flexible segment joint motion errors are assumed to be proportional to the magnitude magnitude of the flexible segment joint motions (in this case we assume a ±20% variation of flexible segment curvature). (a) Two degree-of-freedom interleaved manipulator (flexible segment) workspace. (b) Contour plot of rigid-link joints #1 required RoM over complete workspace. (c) Contour plot of rigid-link joints #2 required RoM over complete workspace.

set to 0 degrees (Fig. 5). However, with this arrangement, the defined workspace contains a singularity in the rigid link joint motion Jacobian, J_r. As seen in Fig. 6b and 6c, the required rigid link joint RoM increases significantly in the vicinity of the singularity (lower left of the configuration space). As seen in Fig. 7, the rigid link joint motion bounds are reduced to a single dimension along the curve of rigid link joint singular positions and thus, make compensation of the flexible segment motion errors (via rigid link joint motion) impossible. From these two examples it is clear that the kinematic arrangement chosen will have a significant impact on the achievable performance improvements (in regards to error correction via rigid link joint motions).

In addition to performance improvements, the redundant rigid link joint motion has the potential to increase the overall manipulator dexterity. The primary limitation on the dexterity of flexible manipulators such as robotic catheters is the limited curvature that the structure can assume – above which the flexible segment can experience mechanical failure. With the introduction of interleaved rigid link joints, this limitation can be overcome. While the design space is complex and direct comparison of a flexible-only manipulator to an interleaved design is difficult, it is still instructive to examine the dexterous workspace of a simple planar manipulator. In this example, the flexible segment-only manipulator consists of three equal length serial flexible segments. The total length of the manipulator is 150 mm and the minimum possible flexible segment radius is limited to 45 mm (equivalent to a maximum curvature of 0.022 $^{1}/_{mm}$). The interleaved manipulator consists of two equal length flexible segments with a single rigid link joint (with 90° nominal orientation) interleaved between the proximal and distal flexible segments. The total length of the manipulator and the minimum flexible segment radius are the same as for the flexible-segment only manipulator. In this case, the task is defined by the position of the manipulator end point and orientation of the distal end of the most distal segment. To limit the scope of the analysis, the task is constrained to maintain a horizontal tip orientation. Given the task constraint on orientation, the dexterous workspace of the flexible segment-only manipulator is shown in Fig. 8a.

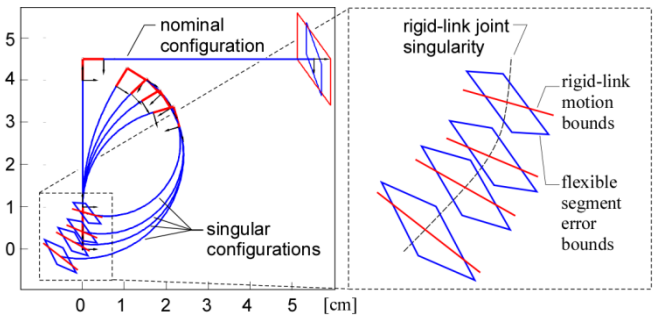

Figure 7. Flexible segment error bounds and rigid-link joint motion bounds drawn along the curve of rigid-link joint singular configurations.

In comparison, the dexterous workspace of the example interleaved manipulator is shown in Fig. 8b. As seen in Fig. 8b, the workspace is a function of the joint range of the rigid link joint. For modest rigid link joint motions (<45°), the dexterous workspace area is comparable to that of the flexible segment-only manipulator. However, as the rigid link joint range of motion is increased, the dexterous

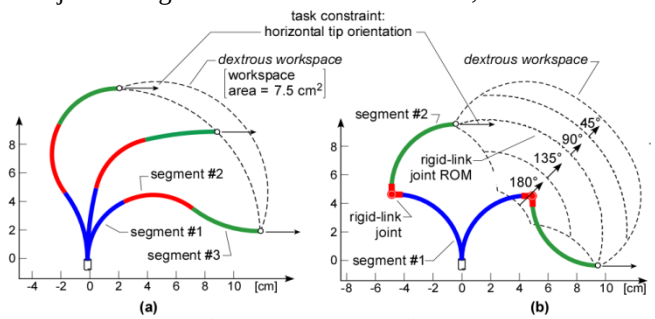

Figure 8. Comparison of dexterous workspace for a simple example three-degree-of-freedom manipulator. (a) Dexterous workspace for example 3-segment flexible manipulator. (b) Dexterous workspace for an example interleaved manipulator (2 flexible segments and one interleaved rigid-link joint) as a function of rigid-link joint range of motion (RoM). Workspaces of 8.6, 20.6, 32.3, and 38.9 cm^2 are spanned by RoMs of ±45, 90, 135, and 180°.

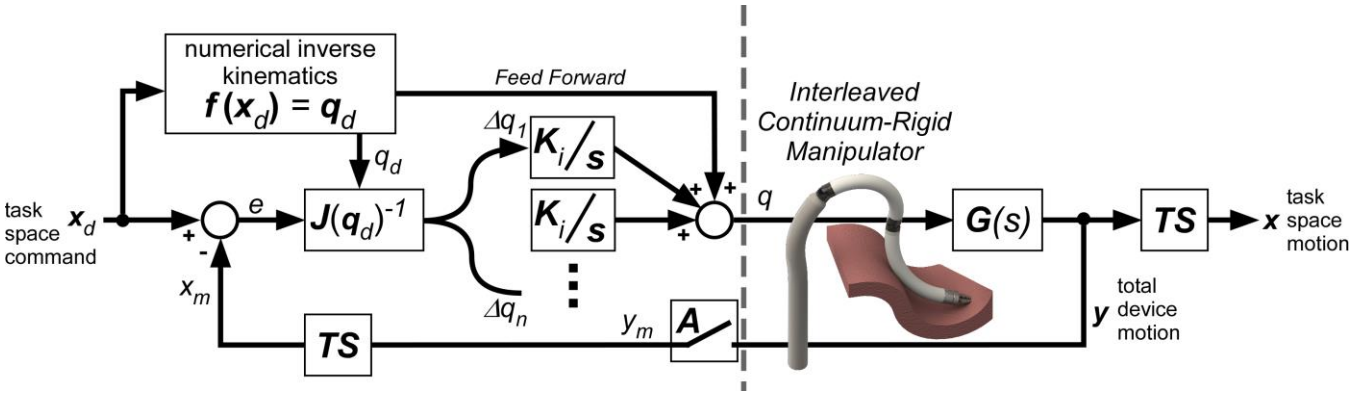

Figure 9. A controller for a large workspace, high accuracy manipulator.

workspace increases significantly. When the rigid link joint range of motion is equal to ±90°, the area of the interleaved manipulator's workspace is almost three times larger than the workspace of the flexible segment only. If the rigid link joint range of motion is increased to ±180°, the ratio of interleaved to flexible segment only workspace area increases to more than 5.

While this is just a representative example (with no consideration for design optimization in regards to relative segment lengths) it does serve to illustrate the potential of the interleaved approach in regards to end-effector dexterity. From the two examples described, it is clear that the effectiveness of the approach is dependent on the kinematic arrangement selected while the requirements on rigid link joint range of motion are directly linked to the kinematic design choices made.

IV. Closed Loop Redundant Control

As mentioned above, many factors can influence the design of an interleaved manipulator which, in turn, greatly affect controller design. Our previous work [2] had a very fast and small range-of-motion rigid joint and a slower, large workspace flexible section. The controller on that system resolved the control redundancy by partitioning the task error into high- and low-frequency components appropriate to each joint, allowing control above the inherent limits of the flexible joint.

The manipulator used in section V has rigid joints that have approximately the same bandwidth and range of motion as the flexible segments. In choosing this design, we were first interested in achieving high accuracy throughout a large workspace, with a secondary interest in control bandwidth.

Given this case, one simple control approach is to explicitly use the rigid link joints to compensate for task error. The full effects of this choice will be discussed in the experimental section, so for now we will focus on the control design as it applies to a general, multiple DoF redundant manipulator. The controller shown in Fig. 9 has a feedforward term for the flexible segment commands and a series of integral controllers for each rigid joint. The feedforward path uses the flexible segment inverse kinematics to find a set of flexible segment joint positions which achieve the given task, x_d. Note that the uniqueness of these joint positions is a function of the task space and inverse kinematics algorithm. The rigid joint position commands are determined by first computing the task space error e from the measured task space position, x_m. This error multiplies the rigid joint subset of the manipulator Jacobian J to find incremental rigid joint positions, Δq. This Jacobian is formed numerically by taking the task-space difference between positive and negative perturbations of the forward kinematics, in the same way that one approximates a derivative numerically. As the rigid joints are generally not identical, each incremental joint command is given to an integral controller with joint-specific gains whose outputs are summed with the initial joint positions from the feedforward path. Fig. 9 assumes no cross-coupling between joints, but were this present it should be considered before the plant $G(s)$. Measurements of the manipulator configuration y_m are converted into the task space x_m to determine the task space error.

In Fig. 9 we do not close the loop around the flexible joints because their motion is difficult to model. Their actuation errors arise from their inherently safe, atraumatic construction. The tendon-actuated catheter is especially frustrating; as has been well documented [6] the tendon/lumen friction leads to nonlinear hysteresis which varies across the workspace. This is difficult to model and can therefore lead to limit cycling; we avoid this by closing the control loop only around the rigid joints.

Another question concerns the computation of the rigid joint Jacobian, which is based on perturbations to the desired joint positions, rather than measured joint positions. This was done for simplicity at the potential cost of robustness, since the alternative requires running the IK on the measured manipulator configuration in the realtime controller and handling convergence failures and occasions when the IK and realtime controller pursue different solutions.

Finally, the experimental manipulator of section V and other similar devices may need to operate across contractions in the null space. This effect can be seen by considering a task outside of the flexible segment range of motion and within that of the rigid joints. In Fig. 9, this has the effect of holding the affected flexible joint at its joint limit and

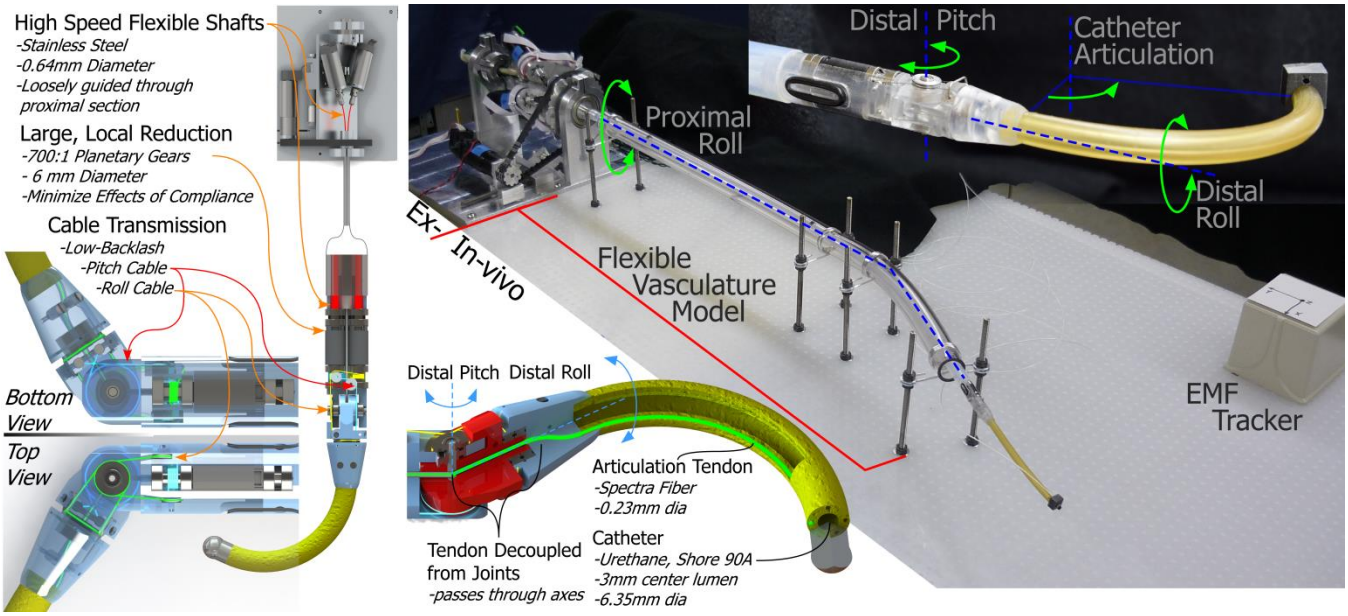

Figure 10. A clinically-relevant prototype system.

pushing the task command onto the task space rigid joint integral controller.

V. Experiment

A. Manipulator Description

The preceding kinematic approach and task space controller were explored on a clinical prototype which has two redundant DoFs. This prototype was described in detail in [1]; the salient features are shown in Fig. 10 and briefly described here.

The manipulator has two flexible segments and two rigid joints; these are arranged so that their ranges of motion overlap to yield two redundant DoFs. All actuators are located outside of the patient, allowing access to high performance servo drives and avoiding the need for drive sterilization. Their motions are communicated through a flexible vasculature model to an interleaved manipulator. The first flexible segment is the non-articulating flexible proximal section which has a roll degree of freedom. This is followed by rigid pitch and roll joints which are remotely actuated by flexible driveshafts. Large reductions in the rigid joints serve to minimize the effects of driveshaft and proximal section compliance, such that no distal encoders are necessary. The output of the local reductions is communicated to the pitch and roll joints via cables; the use of cables enabled a more compact joint design than possible by other transmissions. The second flexible segment follows the pitch and roll joints and consists of a catheter which can be articulated via a tendon routed through the neutral axes of the proximal roll, distal pitch, and distal roll joints and along the periphery of the catheter. This arrangement decouples catheter articulation from the motion of proximal joints, which serves to reduce the effects of friction between the tendon and catheter guide lumen.

In addition to the two flexible and two rigid joints, a fifth, virtual joint was added by projecting along tip pointing vector a variable distance. This projection is based on the catheter pose as measured by an electromagnetic tracker located at the catheter tip. This yields a five DoF manipulator capable of a variety of tasks in 3D and other spaces.

The manipulator singularity of primary importance is the catheter singularity, occurring when the catheter is completely straight. This is an algorithmic singularity, as it is a function of the representation of the catheter pose which, in [2] involves the inverse of the curvature. This singularity is avoided by maintaining a small positive curvature at all times. The other manipulator singularities occur when the projected tip position happens to be near or intersect one of the other joints; these configurations are prohibited by joint limits.

The task controller gains are tuned according to controller configuration and general operating position. A controller tuned to the limit of stability near the neutral axis will be unstable at more highly articulated tasks. (There are several reasons for this which will be touched on while discussing Fig. 12.)

B. Experimental Results

As described above, the aim of this manipulator was to access a large workspace with high task accuracy, with a secondary interest in the response speed. Two 3D circles with twenty steps each were commanded in the global reference frame, with the manipulator tasked to point at each step target, as shown in figure 11.

The circles lie in the space common to both pairs of joints and have approximately 10mm between each step, with a 5 second dwell for convergence before the next step is commanded. The task requires the 3D alignment of the projected tip position to the target circle-point, so in Fig. 9 the task space transformation *TS* strips the manipulator orientation from the pose, leaving only the spatial position.

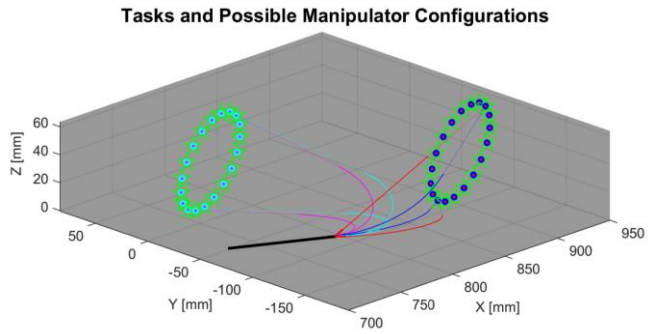

Figure 11. The experimental trajectory consists of two sets of twenty ~10mm step commands which form circles in 3D space. Two manipulator configurations execute each circle command: 'flexible' - blue and cyan - proximal roll, catheter, and projected tip; 'rigid' - red and magenta - proximal roll, distal pitch, distal roll, projected tip. Motion proceeds counterclockwise (as viewed) from the lowermost point. The vasculature model and drives lie at (0,0,0), beyond the lower left of the figure.

Two configurations were demonstrated, the first consisting of the flexible joints – proximal roll, catheter, and projected tip distance – and the second the rigid joints – proximal roll, distal pitch, distal roll, and projected tip distance. The proximal roll was included with the rigid joints because its motion is sufficiently linear to allow closed loop control. In the context of Fig. 9, the named joints form the Jacobian, while all joints are given the feedforward command. In both configurations and for each circle the task gains were tuned iteratively until instabilities were encountered.

Fig. 12 shows the normalized error for each of the configurations executing the two circles. The error is defined as the 3D distance between the commanded position and the position of the projected tip, as measured by an electromagnetic tracker. The projected tip position is determined by measuring the tip position and orientation, and projecting along the tip pointing vector the commanded virtual joint distance.

In both panels the error and manipulator response time are functions of the position on the circle, growing as more motion in the XY plane is required. For these tasks, motion in the Z direction is primarily accomplished by the two roll joints while the XY plane is mostly performed by the pitch and catheter. As mentioned above, the proximal roll joint performance is surprisingly fast and well-modeled by the forward kinematics. For this reason the proximal roll was included in both manipulator controller configurations and its good performance is the reason that steps primarily in Z have less error than primarily in XY.

In Fig. 12 panel a), action at the neutral axis is easily accomplished by both flexible and rigid configurations, taking an average of 0.55 and 0.73 seconds, respectively, to remain within 3mm of the commanded position. The flexible configuration is faster than the rigid because the flexible joint linkages (belt or tendon) are substantially stiffer than the rigid joints whose flexible shafts experience windup. This windup is not presently estimated or corrected in the rigid joint controllers, but certainly can be.

In the lower panel of Fig. 12, the circle requires high articulations. Under the flexible controller the catheter articulates between 130-150°, whereas the neutral task only requires 70° articulations. Articulating catheters suffer a few nonlinear effects at high articulation, principal among these is tendon/lumen friction. This effect described in detail in, for example [6], but for these 130-150° articulations, the joint controller is actually commanding 160-190° articulations. This substantial difference leads to poorer performance due to both a highly nonlinear input/output relationship and errors in the forward kinematics. In Fig. 9, inverse kinematics are not run on the measured manipulator

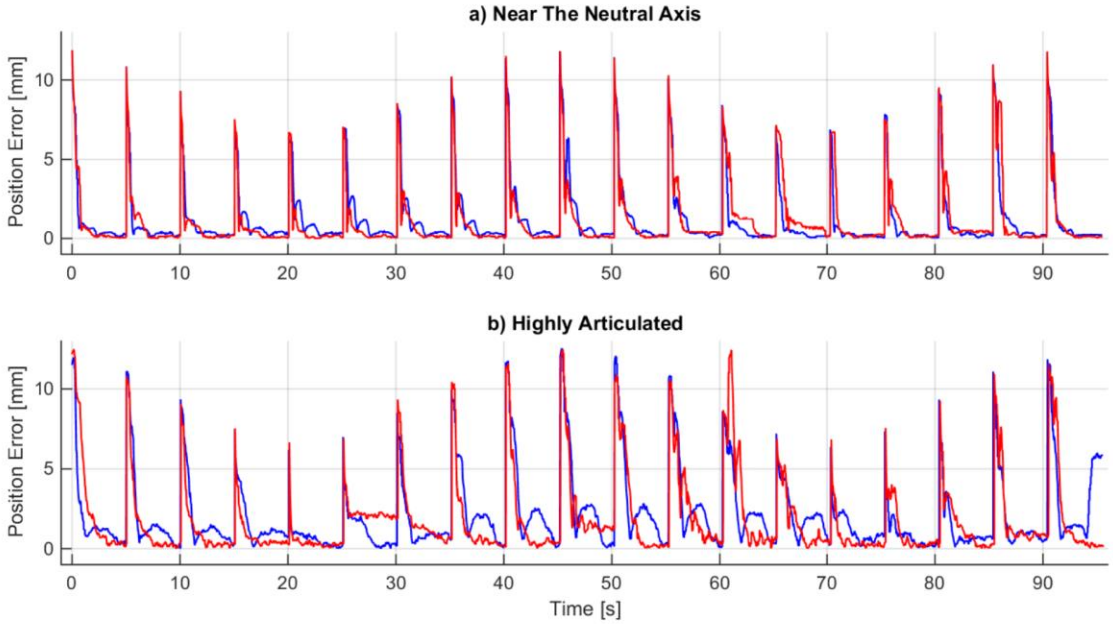

Figure 12. Projected tip position error for the tasks shown in Fig. 11. The flexible configuration has the blue errors, while the rigid is colored red. The first step includes a point move from the neutral position and is therefore omitted. An electromagnetic pose sensor is located on the catheter tip; the virtual joint projects along the measured tip position and orientation the commanded joint distance.

position, allowing the forward kinematics to differ from the actual manipulator state. As the Jacobian is formed from the forward kinematics, this discrepancy leads to joint updates that are not entirely beneficial. This same effect impairs the feedforward path and can result in step motions orthogonal to the intended direction.

As the flexible segments provide access to a large workspace, the rigid controller configuration commands a static articulation to the catheter and therefore experiences a similar discrepancy. In this highly articulated configuration the flexible arrives within 3mm of the target within 1.2 seconds, while the rigid takes only 0.98 seconds. That both times are increased is believed to be due to this forward kinematics discrepancy; the rigid configuration improves relative to the flexible because it does not have the additional friction nonlinearity during refinement. This can be seen in Fig. 12, where the convergence at timesteps 20, 70, and 75 are quite similar. At these times the primary motion is in Z and the catheter or pitch has little to do. In primarily XY motions the rigid joint shows good convergence while the catheter is noticeably delayed.

VI. Concluding Thoughts

To overcome the performance challenges of using flexible continuum manipulators in minimally-invasive surgical procedures we have described a new approach to continuum robotic manipulator design and actuation. Interleaved continuum-rigid manipulation introduces several design freedoms which can be used to substantially improve continuum manipulator performance. The closed loop controller demonstrated here provides great task performance while the kinematic model is close to reality. As the model diverges from reality the task performance decreases; tuning the model to maintain accuracy will be considered going forward. Finally, having demonstrated the task performance of the closed loop controller, our next work will explore redundant controllers in the context of interleaved continuum manipulation.

VII. References

[1] B. L. Conrad and M. R. Zinn, "Interleaved Continuum-Rigid Manipulation Approach: Development and Functional Evaluation of a Clinical Scale Manipulator," in *2014 IEEE/RSJ International Conference On Intelligent Robots and Systems (IROS)*, 2014, pp. 4290–4296.

[2] B. L. Conrad, J. Jung, R. S. Penning, and M. R. Zinn, "Interleaved continuum-rigid manipulation: An augmented approach for robotic minimally-invasive flexible catheter-based procedures," in *2013 IEEE International Conference On Robotics and Automation (ICRA)*, 2013, vol. submitted, pp. 718–24.

[3] "Intuitive Surgical, Inc." [Online]. Available: http://www.intuitivesurgical.com.

[4] "Hansen Medical." [Online]. Available: http://www.hansenmedical.com/international/products/ep/artisan-control-catheter.php.

[5] Stereotaxis, "Niobe Magnetic Navigation System." [Online]. Available: http://www.stereotaxis.com/physicians/the-lab/components/niobe-es/.

[6] J. Jung, R. S. Penning, N. J. Ferrier, and M. R. Zinn, "A Modeling Approach for Continuum Robotic Manipulators: Effects of Nonlinear Internal Device Friction," in *2011 IEEE/RSJ International Conference On Intelligent Robots And Systems (IROS)*, 2011, pp. 5139–5146.

[7] R. S. Penning, J. Jung, N. J. Ferrier, M. R. Zinn, and S. Paul, "An Evaluation of Closed-Loop Control Options for Continuum Manipulators," in *2012 IEEE International Conference On Robotics and Automation (ICRA)*, 2012, pp. 5392–5397.

[8] P. E. Dupont, J. Lock, B. Itkowitz, and E. Butler, "Design and Control of Concentric-Tube Robots," *IEEE Trans. Robot.*, vol. 26, no. 2, pp. 209–225, Apr. 2010.

[9] R. J. Webster, J. P. Swensen, J. M. Romano, and N. J. Cowan, "Closed-Form Differential Kinematics for Concentric-Tube Continuum Robots with Application to Visual Servoing," in *Experimental Robotics*, O. Khatib, V. Kumar, and G. J. Pappas, Eds. Springer Berlin Heidelberg, 2009, pp. 485–494.

[10] R. J. Webster, J. M. Romano, and N. J. Cowan, "Mechanics of Precurved-Tube Continuum Robots," *IEEE Trans. Robot.*, vol. 25, no. 1, pp. 67–78, 2009.

[11] H. Choset and W. Henning, "A follow-the-leader approach to serpentine robot motion planning," *J. Aerosp. Eng.*, vol. 12, no. April, pp. 65–73, 1999.

[12] A. Degani, H. Choset, A. Wolf, T. Ota, and M. A. Zenati, "Percutaneous Intrapericardial Interventions Using a Highly Articulated Robotic Probe," *First IEEE/RAS-EMBS Int. Conf. Biomed. Robot. Biomechatronics, 2006. BioRob 2006.*, pp. 7–12, 2006.

[13] A. Degani, H. Choset, A. Wolf, and M. A. Zenati, "Highly articulated robotic probe for minimally invasive surgery," in *IEEE International Conference on Robotics and Automation*, 2006, vol. 2008, no. May, pp. 3273–6.

[14] R. S. Penning, J. Jung, J. A. Borgstadt, N. J. Ferrier, M. R. Zinn, and M. R, "Towards closed loop control of a continuum robotic manipulator for medical applications," in *2011 IEEE International Conference on Robotics and Automation*, 2011, pp. 4822–4827.

[15] S. G. Yuen, D. T. Kettler, P. M. Novotny, R. D. Plowes, and R. D. Howe, "Robotic Motion Compensation for Beating Heart Intracardiac Surgery.," *Int. J. Rob. Res.*, vol. 28, no. 10, pp. 1355–1372, Oct. 2009.

[16] M. Mahvash and P. E. Dupont, "Stiffness control of surgical continuum manipulators," *Robot. IEEE Trans.*, vol. 27, no. 2, pp. 334–345, 2011.

[17] D. B. Camarillo, C. R. Carlson, and J. K. Salisbury, "Configuration Tracking for Continuum Manipulators With Coupled Tendon Drive," *IEEE Trans. Robot.*, vol. 25, no. 4, pp. 798–808, Aug. 2009.

[18] K. Xu, S. Member, and N. Simaan, "An Investigation of the Intrinsic Force Sensing Capabilities of Continuum Robots," *IEEE Trans. Robot.*, vol. 24, no. 3, pp. 576–587, Jun. 2008.

[19] F. Arai, M. Ito, T. Fukuda, M. Negoro, and T. Naito, "Intelligent assistance in operation of active catheter for minimum invasive surgery," *Proc. 1994 3rd IEEE Int. Work. Robot Hum. Commun.*, pp. 192–197, 2002.

[20] Y. Bailly, a. Chauvin, and Y. Amirat, "Control of a high dexterity micro-robot based catheter for aortic aneurysm treatment," *IEEE Conf. Robot. Autom. Mechatronics, 2004.*, vol. 1, pp. 65–70, 2004.

[21] V. K. Chitrakaran, A. Behal, D. M. Dawson, and I. D. Walker, "Setpoint regulation of continuum robots using a fixed camera," in *American Control Conference*, 2004, pp. 1504–1509.

[22] K. Xu and N. Simaan, "Actuation compensation for flexible surgical snake-like robots with redundant remote actuation," in *International Conference on Robotics and Automation*, 2006, no. May, pp. 4148–4154.

[23] A. Bajo, N. Simaan, and S. Member, "Kinematics-Based Detection and Localization of Contacts Along Multisegment Continuum Robots," *IEEE Trans. Robot.*, vol. 28, no. 2, pp. 291–302, 2012.

[24] N. Simaan, K. Xu, A. Kapoor, W. Wei, P. Kazanzides, P. Flint, and R. Taylor, "Design and Integration of a Telerobotic System for Minimally Invasive Surgery of the Throat.," *Int. J. Rob. Res.*, vol. 28, no. 9, pp. 1134–1153, Sep. 2009.

[25] J. Jayender, M. Azizian, and R. V. Patel, "Autonomous image-guided robot-assisted active catheter insertion," *IEEE Trans. Robot.*, vol. 24, no. 4, pp. 858–871, 2008.

[26] J. Jayender, R. V. Patel, and S. Nikumb, "Robot-assisted Active Catheter Insertion: Algorithms and Experiments," *Int. J. Rob. Res.*, vol. 28, no. 9, pp. 1101–1117, May 2009.

[27] M. W. Spong, S. Hutchinson, and M. Vidyasagar, *Robot Modeling and Control*. Hoboken, NJ: John Wiley & Sons, Ltd, 2006.